Acta Geochim (2023) 42:971–987
https://doi.org/10.1007/s11631-023-00623-9

ORIGINAL ARTICLE

Geochemistry of the Aptian bituminous limestones in Gümüşhane area, Eastern Black Sea region: new insight into paleogeography and paleoclimate conditions

Merve Özyurt[1]

Received: 14 February 2023 / Revised: 6 June 2023 / Accepted: 14 June 2023 / Published online: 24 August 2023

Abstract Aptian is characterized by widespread deposition of organic-rich sediment. The Aptian bitumen limestone horizon, which is thin decimetre-thick sequences, locally crops out in the Kırcaova area, Eastern Black Sea Region (Eastern Pontides). They are well correlated with Aptian bitumen limestone in the other Tethys Reams. They are proposed as episodes of increased organic matter. However, background factors controlling organic matter enrichment are poorly known. In this study, we present new inorganic geochemistry, including trace elements, rare earth elements (REE), redox-sensitive elements (RSE), stable-isotopes ($\delta^{18}O$ and $\delta^{13}C$), and total organic carbon (TOC). We integrated new geochemical data with existing stratigraphy, paleontology, and organic chemistry data to provide new insight into the depositional environment and paleoclimate conditions during Aptian. The lacustrine bitumen limestone (LBL) samples have varied $\delta^{13}C$ (ave. -1.45‰) and $\delta^{18}O$ (ave.-4.50‰). They possess distinct REE patterns, with an average of REE (ave. 14.45 ppm) and Y/Ho (ave. 35) ratios. In addition, they have variable Nd/Yb_N (0.28–0.81; ave. 0.56) and Ce/Ce* (0.68–0.97; ave. 0.86), and relatively high Eu*/Eu (1.23–1.53; ave. 1.35). They display seawater signatures with reduced oxygen conditions. The enrichment in RSE (Mo, Cu, Ni, and Zn) and the low Mo/TOC (0.70–3.69; ave. 2.41) support a certain degree of water restriction. The high Sr/Ba, Sr/Cu, Ga/Rb, and K/Al records of the LBL facies suggest hot house climatic conditions. The sedimentary environment was probably an isolated basin that is transformed from the marine basin. In addition to depositional conditions, the regional parameters such as the climate, increased run-off period, nutrient levels, alkalinity level, and dominant carbonate producers favored the enrichment in organic matter of LBL facies. Thus, extreme greenhouse palaeoclimate conditions have an important role in organic matter enrichment in the isolated basin. Our results are conformable with the published data from marine, semi-restricted basin, and lacustrine settings in the different parts of the Tethys margin. Thus, this approach provides the first insight into the Aptian greenhouse paleo-climate conditions of the Eastern Black Sea Region, NE Turkey.

Keywords Aptian · Paleoclimate · Sedimentary conditions · Geochemistry · REE · C and O isotopes · Limestone · Eastern Black Sea

1 Introduction

Lacustrine carbonates are widely exposed all over the world and serve as significant archives of Earth's history. They usually host a wide spectrum of hydrocarbon deposits. The enrichment of organic matter in sediments is an important biogeochemical process and it can be associated with not only the paleoenvironmental conditions such as temperature and oxygenation level but also with the primary source (Arthur and Sageman 1994; Burdige 2007). Several hypotheses have been proposed to understand their genesis which is still hotly debated. Two commonly discussed models are the preservation (e.g., Demaison and Moore 1980; Arthur and Sageman 1994; Mort et al. 2007) and the productivity (e.g., Pedersen and Calvert 1990;

✉ Merve Özyurt
merveyildiz@ktu.edu.tr

[1] Geological Engineering Department, Karadeniz Technical University, Ortahisar, Trabzon TR-61080, Turkey

Sageman et al. 2003) models. In the preservation model, the isolation of the benthic environment beneath a permanent pycnocline leads to bottom water anoxia. A modern example of this is the Black Sea, organic matter preservation occurs under conditions of balanced diminution and/or lack of aerobic decomposition. On the other hand, the productivity model relates to increases in primary productivity in surface waters, which subsequently result in elevated benthic oxygen demand exceeding its resupply through water column mixing in the natural system (Murphy et al. 2000). However, recently a great amount of research has highlighted the influence of other processes such as clastic input, weathering processes, climatic conditions, water-level fluctuations, and water circulation on the sequestration of organic matter (e.g., Sageman et al. 2003; Rimmer 2004; Riquier et al. 2006). Advancements in sedimentology have provided new clues into the background controls for the deposition of organic-rich carbonates. Nowadays, the rare earth elements (REEs) contents of carbonates have been widely used by sedimentologists to asses syn-sedimentary conditions and diagenetic paragenesis of extensive carbonate bodies (Nothdurft et al. 2004; Frimmel 2009; Özyurt et al. 2020; Gong et al. 2021). In addition, the REE chemistry of carbonates has proven to be an important proxy for constraining the tectonic setting of sedimentary basins (Bau 1991, 1996; Nothdurft et al. 2004; Zhang et al. 2017; Özyurt et al. 2020, 2023; Satish-Kumar et al. 2021).

The rare earth elements (REEs), as coherent series of elements, exhibit similar physical–chemical behaviors in a natural aqueous system, but the abundances of REEs (from Lu to La) are preferentially fractionated along the series, resulting in the preferential removal of the light REEs (LREE) compared to the heavy REEs (HREE) in seawater (e.g., Sholkovitz et al. 1994; Sholkovitz and Shen 1995; Byrne and Sholkovitz 1996). Generally, REEs exist in stable trivalent (3 +) oxidation states, with the exceptions of Ce (Ce^{3+}, Ce^{4+}) and Eu (Eu^{2+}, Eu^{3+}), which can be formed as multivalent under different redox states of the natural system (Elderfield 1988). The redox state of seawater controls the oxidization of Eu and reduction of Ce (Bau 1991). Under anoxic conditions, depletion of the Ce can be weakened due to the redox reactions, oxidizing Ce^{3+} to insoluble Ce^{4+}. Thus dissolved Ce^{3+} is partially scavenged from seawater (German and Elderfield 1989; de Baar et al. 1991; Koeppenkastrop and Eric 1992; Sholkovitz et al. 1994). Hence, the fractionation and distribution of REE and Y in carbonates can be important proxies for paleoenvironmental conditions of depositional environments (Bau 1996; Webb and Kamber 2000; Franchi 2018; Redivo et al. 2019; Liu et al. 2019; Özyurt et al. 2020, 2023). In addition, the REE indices, which are integrated with sedimentological data, C/O isotopes and TOC contents, can deepen our understanding of the paleoenvironmental factors controlling the enrichment of organic matter. During the Early Aptian to Albian, the Eastern Pontide Basin (EPB), northeastern Türkiye, was predominantly characterized by the deposition of outer platforms to slope facies. Although the Aptian records an episode of environmental change from the inner platform to the outer platform (Özyurt et al. 2020, 2022). However, there are exceptional occurrences of Aptian laminated black limestone, known as lacustrine bituminous limestone (LBL) in the Kırcaova of the Eastern Black Sea region (Kara-Gülbay et al. 2012). The LBL facies is described as an Aptian bitumen horizon, which can be correlated with other Tethys Realms, including Slovenia, Greece, and Germany (Kırmacı et al. 1996; Koch and Zimmerle 1996; Koch et al. 2008). Therefore, the LBL strata have the potential to record paleogeography and paleo-climate controls of the organic matter enrichment in the lacustrine basin of Eastern Pontides (NE Turkey). However, detailed inorganic chemistry data for these strata remain largely unexplored, except for organic geochemistry, sedimentology, and paleontological data (Kırmacı et al. 1996; Koch and Zimmerle 1996; Koch et al. 2008; Kara-Gülbay et al. 2012). Therefore, we present the new geochemical data set (C/O isotope, trace elements including RSE, REE) to reveal new implications for the paleo-environment (salinity, paleoredox, clastic flux) and paleo-climate conditions.

1.1 Stratigraphy

The Variscan orogeny in the Black Sea region shares many similarities with Central Europe (Okay and Topuz 2017). However, the tectono-sedimentary evolution of the Tethys in the Eastern Black Sea Region is complicated (Okay and Şahintürk 1997; Okay and Nikishin 2015). The Eastern Black Sea region (Eastern Pontides) is mainly divided into two subzones, including the Northern and Southern Zone based on the distribution of different rock associations (Okay and Şahintürk 1997). The Northern Zone is dominantly composed of the late Cretaceous and middle Eocene volcanic and volcaniclastic rocks, whereas Southern Zone mainly consists of Mesozoic to Eocene sedimentary rocks (Okay and Şahintürk 1997; Şen 2007; Temizel et al. 2012). The Hercynian basement rocks in the Eastern Pontides comprise a pre-Carboniferous high-degree metamorphic complex, an early Carboniferous granodiorite-dacite complex, Late Carboniferous–Early Permian shallow-water clastic sedimentary sequences, and a Permo-Triassic metabasic phyllite-marble unit (e.g. Okay and and Şahintürk 1997, Topuz et al. 2007; Kaygusuz et al. 2012). These heterogeneous basement rocks are overlain by the Early–Middle Jurassic volcano-sedimentary succession (e.g. Sengör et al. 1980; Görür 1988; Kandemir and Yılmaz

2009; Dokuz et al. 2010). The succession shows variations in thickness, ranging from 2 to 1500 m, and consists mainly of conglomerates, sandstone, coal seams, basalt-andesite and pyroclasts, marl, claystone, siltstone, sandstone, micritic limestone alternations, and red limestone with Ammonitico-Rosso facies (Okay and Şahintürk 1997; Kandemir and Yılmaz 2009). The highly variable thickness within a short distance indicates rift-related topography (Kandemir and Yılmaz 2009; Kandemir et al. 2022). During the Late Jurassic–Early Cretaceous, Eastern Pontides witnessed a relatively stable tectonic regime and equatorial–subequatorial paleoclimate conditions, which facilitated to deposition of the platform carbonates (Görür 1988; Kırmacı et al. 1996, 2018; Okay and Sahintürk 1997; Taslı 1991, 1997, 1999; Koch et al. 2008; Özyurt 2019; Özyurt et al. 2019a, b, c). These carbonates display a wide range of microfacies, ranging from supratidal to slope (e.g., Kırmacı et al. 1996; Koch et al. 2008; Özyurt et al. 2020; 2022). Although, the age of the Berdiga Fm. carbonates remain debated due to a paucity of biostratigraphic marker species (Vincent et al. 2018). Numerous Earth scientists have variously proposed that sedimentation started in the Aalenian-Bajocian (Pelin 1977), Callovian (Robinson et al. 1995), Oxfordian or latest Oxfordian (Koch et al. 2008; Akdoğan et al. 2018), Kimmeridgian (Dokuz and Tanyolu 2006; Taslı et al. 1999). In recent studies, the upper part is represented by allochthonous bioclastic wackestone with chert nodules and it is usually assigned to the Aptian-Albian (Taslı 1991; Kırmacı et al. 1996; Koch et al. 2008; Özyurt et al. 2020, 2022). The extensional tectonic regime triggered the drowning of the carbonates and influenced the sedimentation on the Berdiga carbonate platform during the Cretaceous in time and space (Eren and Tasli 2002; Taslı et al. 1999). The erosion or hard ground structure developed on the structural heights, and sedimentation continued until the Cenomanian or Turonian (Pelin 1977; Eren and Tasli 2002; Özyurt et al. 2023). During the extensional regime, the transitional environment has turned into an isolated basin on the structural high area. The Aptian laminated thin-bedded black limestones are deposited in an isolated basin, which is transformed from a lagoon environment. These Aptian laminated thin-bedded black limestones locally occur in the uppermost part of the Berdiga Fm. (Kırmacı et al. 1996; Kara-Gülbay et al. 2012; Özyurt et al. 2020, 2022). Overlying the Berdiga Formation, the Upper Cretaceous sedimentary sequence is mainly composed of deep-marine lithofacies with interbedded volcaniclastics. The lower part of the sequence is represented by yellowish-colored calcirudite, calcarenite, calcilutite, and sandy limestone (Kındıralık dere Fm.; Pelin 1977). The sediments pass upward into the thin-bedded Globutuncana-bearing pelagic limestones, marly limestone, and marl (Elmalı dere Fm.; Pelin 1977). The upper part of the sequence is composed of sandstone, siltstone, marl, clayey limestone, and volcaniclastics (Tepeköy Fm.; Pelin 1977). This Late Cretaceous sedimentary sequence is described as rift sediment due to (1) rapid lateral changes in facies and thickness and (2) hardground structures within the sequence (Eren and Tasli 2002; Kandemir and Yılmaz 2009; Türk-Öz and Özyurt 2019; Özyurt et al. 2023). The sedimentary sequence changes into magmatic rocks, including basalt, andesite, dacite, rhyolite, and, pyroclastics, and a wide range of intrusive rocks, toward the northern part of the Eastern Pontides (e.g., Kaygusuz and Aydınçakır 2009; Karslı et al. 2010). The Upper Cretaceous rocks are cut or overlain by basalt-andesite and associated pyroclastic rocks and Nummulite-bearing limestone of the Eocene Alibaba Formation (Arslan and Aliyazıcıoğlu 2001; Kaygusuz et al. 2009; 2012; Eyuboglu et al. 2013).

2 Samples and methods

The Upper Jurassic–Lower Cretaceous carbonates are widely exposed in the Eastern Pontides, particularly in the southern part. However, the bituminous limestone strata of the Berdiga Formation are rarely preserved in the Eastern Pontides. One of the typical exposures of LBL strata is found in the Kırcaova area of the southern part. The studied stratigraphic section is represented by a 6 m thick, dark grey-colored micritic limestone. Twelve outcrop samples are collected from a 6-m-thick section. Well-preserved micritic limestone samples were selected for detailed trace element and isotope analyses. They were examined under a polarising microscope to determine the microfacies. Microfacies types were described based on Dunham (1962) and interpreted according to Flügel (2012). Representative thin sections and a mirror-image slab of each thin section were polished to evaluate (i) weathering (ii) the presence of clay minerals (iii) micro-fissures filled with calcites or clastic components and (iv) fracturing during geochemical sampling. We selected the most representative LBL samples that do not display petrographic evidence of diagenetic alteration, recrystallization, cementation, secondary minerals, or autogenetic minerals such as glauconite. Their micritic ortho-chem parts were carefully sampled by using the micro-drilling method.

The stable isotope analyses ($\delta^{18}O$ and $\delta^{13}C$) were conducted at the Sedimentary laboratories of the University of Windsor (ON, Canada). Carbonate powders were reacted with 100% phosphoric acid at 70 °C using a Gasbench II connected to a Thermo Fisher Delta V Plus mass spectrometer. All values are reported per mil relative to V-PDB. Reproducibility and accuracy were monitored by replicate analysis of laboratory standards calibrated by assigning

$\delta^{13}C$ values of + 1.95‰ to NBS19 and -46.6‰ to LSVEC and $\delta^{18}O$ values of -2.20‰ to NBS19 and -23.2‰ to NBS18. Reproducibility for $\delta^{13}C$ and $\delta^{18}O$ was ± 0.0 × and ± 0.0y (1 SD), respectively.

Major and trace element analyses of the selected samples were conducted by ACME Analytical Laboratories, Ltd. (Canada). Major elements were analyzed by X-ray fluorescence in fused $LiBO_2/Li_2B_4O_7$ disks using a Siemens SRS-3000 X-ray fluorescence spectrometer with an Rh-anode X-ray tube as a radiation source. X-ray absorption/enhancement effects were corrected using the Traill and Lachance (1966) method, included in the SRS-3000 software. The detection limit was 0.01% for SiO_2, CaO, Al_2O_3, Na_2O, K_2O, MnO, P_2O_5, and TiO_2: 0.04% for Fe_2O_3, and 0.002% for Cr_2O_3. Trace element content including rare earth elements (REE), and redox-sensitive elements (RSE) in the carbonates was determined by inductively coupled plasma–mass spectrometry (ICP–MS). Analyses used ~ 0.2 g of powdered sample digested in 10 mL 8 N HNO_3, of which 1 mL was diluted with 8.8 mL deionized water and 0.1 mL HNO_3. To monitor the precision and accuracy, 1 mL of an internal standard (including Bi, Sc, and In) was added to the solution. For more details on these methods, please see the website of http://acmelab.com. Detection limits for Ba, Ni, and Sc are 1, 20, and 1 μg/g, respectively. Detection limits for Hf, Zr, Y, La, and Ce are 0.1 μg/g. Detection limits for Th and Nd are 0.2 and 0.3 μg/g, respectively. Detection limits for Tm, Tb, and Lu are 0.01 μg/g; for Pr, Eu, and Hu are 0.02 μg/g; for Er is 0.03 μg/g; for Sm, Gd, Dy, and Yb are 0.05 μg/g. $\sum$REE or total REE content includes rare earth elements from La to Lu and Y are separately illustrated in Table 1. $Ce_N/Ce_N* = Ce_N/(0.5La_N + 0.5Pr_N)$; $Eu_N/Eu_N* = Eu_N/[(Sm_N \times 0.67) + (Tb_N \times 0.33)]$, where N refers to normalization to post-Archean Australian Shale (PAAS-normalized value) (Taylor and McLennan 1985). The equations of (i) Eu/Eu* ratio = $Eu_N/(Sm_N + Gd_N)0.5$, (ii) Pr anomaly = Pr/Pr* = $Pr_N/(0.5Ce_N + 0.5Nd_N)$, (iii) La anomaly = La/La* = $La_N/(3Pr_N - 2Nd_N)$, and (iv) Ce anomaly = Ce/Ce* = $3Ce_N/(2La_N + Nd_N)$ are used to express Eu, Pr, La, and Ce anomalies in the studied limestones (Bau and Dulski 1996; Shields and Stille 2001).

3 Results

The underlying facies are represented by reworked skeletal grainstone/packstone microfacies and sponge spicule wackestone/mudstone microfacies. The studied strata overlie the underlying facies with a sharp contact, which implies disconformity. The LBL facies are composed of thin to medium layered, black to dark gray bituminous limestones and clayey limestone layers. The lower part is represented by thin to medium layered, bioclastic wackestone, whereas the middle to upper levels comprises thin to very thin bedded, bioclastic lime mudstone that intercalated with clayey limestone. The samples contain gastropod, ostracod, and characean stems, and benthic foraminifera such as miliolid. Koch and Zimmerle (1996) indicated that Aptian LBL forms a marker horizon in the field (Figs. 1, 2, 3, 4).

3.1 Stable isotopes ($\delta^{18}O$ and $\delta^{13}C$)

Their stable isotopes ($\delta^{18}O$ and $\delta^{13}C$) are illustrated in Table 1. The $\delta^{13}C$ values of the bituminous limestone samples ranging from − 2.19‰ to − 0.90 ‰ with an average of -1.45 ‰ are slightly lower than those of the Belemnite shells (0.10 and 1.84 ‰). The $\delta^{18}O$ data (-4.90 to -3.53 with ave. -4.50) are slightly lower than those of belemnite fossils (-3.49 to -1.75, with an average of -2.75; Özyurt et al. 2022).

3.2 Major-trace elements and TOC values

Major, trace, and rare earth elements are presented in Tables 1 and 2. The studied samples show similar $CaCO_3$ contents ranging from 98.71 to 99.38 wt.%. They exhibit low-Mg calcite characteristics with $MgCO_3$ values between 0.62 and 1.29 wt.%. They have significantly high Fe (0.19–0.88 wt.% with ave. 0.56%) and high Mn (0.05–0.20 wt.% with ave. 0.10 wt.%) and variable Na (0.01–0.02%) contents. Further, they have relatively high Sr (499–879 ppm; average 712 ppm). They have total carbon (12.06 to 13.17 wt.%, with ave. 12.39 wt.%), total organic carbon (TOC; 0.43 to 1.46 wt.%, with ave. 0.78 wt.%), and total S content (0.03–0.11 wt.%, with ave. 0.05 wt.%). They exhibit low Zr, Sc, Hf, and Sc contents. Their redox-sensitive trace elements (RSE; Mo, Cu, Ni, and Zn) are represented in Table 2. The total rare earth elements ($\sum$REE) of bituminous limestone samples range from 2.68 to 39.90 ppm (ave. of 12.80 ppm), which are higher than the REE concentrations of belemnite samples (0.32–0.54). The average $\sum$REE contents in the bituminous limestone samples are significantly low compared to those in the Post-Archean Australian Shale (PAAS) (183 ppm; Taylor and McLennan 1985), North American Shale Composite (NASC) (173 ppm; Boynton 1984). They have chondritic Y/Ho ratios varying between 29.17 and 50.00 with an average of 35. The normalized REE patterns display LREE depletion relative to the HREEs (ave. 0.62 of La/YbN and mean 0.54 of Nd/YbN); positive La anomaly (ave. 2.82 of La*/La); positive Eu anomaly (Eu/Eu*; 1.23–1.53, with ave. 1.34); and slightly flattened Ce anomaly (Ce/Ce*;0.68–0.97, with ave. 0.88) (Fig. 5).

Table 1 Trace element and isotope values of the studied LBL strata. Bdl: Below detection limit

Sample	LBL-1	LBL-2	LBL-3	LBL-4	LBL-5	LBL-6	LBL-7	min	max	ave
$\delta^{13}C$	−2.19	−1.50	−1.10	−2.10	−0.90	−0.91	−1.10	−2.19	−0.90	−1.40
$\delta^{18}O$	−3.53	−4.66	−4.20	−4.40	−4.90	−4.50	−4.70	−4.90	−3.53	−4.50
SiO_2	0.96	0.67	0.66	0.60	3.21	2.75	4.16	0.60	4.16	1.86
Al_2O_3	0.25	0.15	0.15	0.16	0.95	0.84	1.34	0.15	1.34	0.55
Fe_2O_3	0.38	0.76	0.78	0.19	0.58	0.37	0.88	0.19	0.88	0.56
MgO	0.83	0.92	0.93	1.02	0.74	0.80	0.82	0.74	1.02	0.87
CaO	53.65	53.64	53.60	53.85	51.29	51.25	50.36	50.36	53.85	52.52
Na_2O	0.02	0.02	0.02	0.02	0.02	0.01	0.02	0.01	0.02	0.02
K_2O	0.04	0.02	0.02	0.02	0.13	0.10	0.19	0.02	0.19	0.07
TiO_2	0.01	bdl	bdl	bdl	0.05	0.04	0.07	0.01	0.07	0.04
P_2O_5	0.03	0.02	0.03	0.03	0.05	0.04	0.03	0.02	0.05	0.03
MnO	0.20	0.14	0.14	0.05	0.05	0.05	0.05	0.05	0.20	0.10
Ba	8.00	11.00	14.00	9.00	18.00	21.00	19.00	8.00	21.00	14.29
Sc	bdl	bdl	bdl	bdl	1.00	bdl	2.00	1.00	2.00	1.50
LOI	43.50	43.60	43.60	43.90	42.80	43.60	41.90	41.90	43.90	43.27
Sum	99.92	99.91	99.90	99.89	99.88	99.88	99.88	99.88	99.92	99.89
Co	0.50	0.50	0.20	0.50	2.20	1.80	2.20	0.20	2.20	1.13
Cs	0.20	0.10	0.20	0.20	1.70	1.20	1.80	0.10	1.80	0.77
Ga	0.50	0.50	0.50	0.60	1.20	0.70	1.40	0.50	1.40	0.77
Hf	bdl	bdl	bdl	bdl	0.20	0.20	0.30	0.20	0.30	0.23
Nb	0.20	0.20	0.10	0.10	0.80	0.60	0.90	0.10	0.90	0.41
Rb	1.90	1.30	1.10	1.20	5.30	4.40	8.20	1.10	8.20	3.34
Sr	499	623	629	706	801	879	765	499	879	700
U	1.80	1.80	1.80	2.50	4.30	4.60	3.00	1.80	4.60	2.83
V	8.00	8.00	10.00	15.00	24.00	23.00	31.00	8.00	31.00	17.00
Zr	3.40	3.20	3.00	9.70	8.40	7.00	11.20	3.00	11.20	6.56
Y	1.90	1.00	1.10	12.30	2.10	1.30	3.50	1.00	12.30	3.31
La	1.10	0.70	0.60	5.60	2.00	1.50	3.50	0.60	5.60	2.14
Ce	1.60	0.80	1.00	7.90	3.40	2.50	5.30	0.80	7.90	3.21
Pr	0.18	0.11	0.10	0.91	0.35	0.26	0.61	0.10	0.91	0.36
Nd	0.50	0.50	0.50	4.20	1.50	1.30	2.50	0.50	4.20	1.57
Sm	0.13	0.09	0.07	1.19	0.37	0.17	0.48	0.07	1.19	0.36
Eu	0.04	0.03	0.03	0.37	0.08	0.06	0.13	0.03	0.37	0.11
Gd	0.21	0.13	0.18	1.91	0.28	0.24	0.52	0.13	1.91	0.50
Tb	0.03	0.02	0.02	0.30	0.04	0.03	0.07	0.02	0.30	0.07
Dy	0.27	0.11	0.13	1.95	0.32	0.19	0.50	0.11	1.95	0.50
Ho	0.05	0.02	0.03	0.42	0.07	0.04	0.12	0.02	0.42	0.11
Er	0.18	0.09	0.10	1.27	0.21	0.14	0.30	0.09	1.27	0.33
Tm	0.02	0.01	0.01	0.19	0.03	0.02	0.04	0.01	0.19	0.05
Yb	0.14	0.07	0.09	1.20	0.17	0.13	0.29	0.07	1.20	0.30
Lu	0.03	0.01	0.01	0.19	0.02	0.02	0.04	0.01	0.19	0.05
TOT/C	12.23	12.21	12.31	12.42	12.35	13.17	12.06	12.06	13.17	12.39
TOT/S	0.03	0.03	0.03	0.04	0.05	0.11	0.07	0.03	0.11	0.05
TOC	0.71	0.48	0.45	0.43	1.11	1.46	0.84	0.43	1.46	0.78
Mo	0.70	1.50	1.20	0.30	4.10	4.20	2.60	0.30	4.20	2.09
Cu	1.20	1.20	1.40	0.80	4.90	3.50	5.80	0.80	5.80	2.69
Pb	0.60	0.40	0.40	0.30	1.40	0.90	2.50	0.30	2.50	0.93
Zn	2.00	3.00	3.00	1.00	7.00	6.00	12.00	1.00	12.00	4.86
Ni	2.80	4.20	4.10	0.90	7.60	4.40	7.80	0.90	7.80	4.54

TOT/C Total carbon. *TOT/S* Total sulfur

4 Discussion

4.1 Clastic influx

The REE composition of carbonate can be easily influenced by non-carbonate materials, which contain relatively high REE concentrations. These non-carbonate materials mainly include terrigenous detritus (Webb and Kamber 2000; Nothdurft et al. 2004; Frimmel 2009), Fe–Mn oxides (Banner et al. 1988; Bau 1996; Frimmel 2009) and phosphates (German and Elderfield 1990; Reynard et al. 1999). In addition, organic matter can also absorb REE contents. The presence of a non-carbonate component can be detected through insoluble elements such as Sc, Th, and Hf, which are enriched in terrigenous detritus such as clay minerals (Webb and Kamber 2000; Özyurt et al. 2020). Firstly, the ΣREE concentrations of the LBL samples are lower than those of terrigenous sediments (marine carbonate is usually < 100 ppm, Qing and Mountjoy 1994; Li et al. 2017). Their ΣREE concentrations are in accordance with shallow marine carbonates (Özyurt et al. 2020). Although Y/Ho ratios display chondritic values (29–50) which are lower than marine carbonates. The studied LBL samples have significantly lower mean concentrations of Sc, Th, and Hf compared to the upper crust (i.e., Sc = 14.9 ppm, Th = 2.30 ppm, Hf = 5.80 ppm; Taylor and Mclennan 1985).

4.2 Depositional environment

The LBL facies is represented by black to dark gray bituminous limestones and clayey limestone. These facies are described as an Aptian bitumen horizon (Kırmacı et al. 1996; Koch and Zimmerle 1996). The LBL facies in Eastern Pontides are well correlated with the bituminous limestone in W-Slovenia based on paleontological and stratigraphical data (Koch and Zimmerly 1996). Although, the shallow-marine index fossils of the bitumen horizon in Eastern Pontides differ from those in W-Slovenia. In both areas, the bituminous limestone strata contain characeans, indicating periodic deposition in a freshwater environment (Koch and Zimmerly 1996; Kırmacı et al. 1996). Previous studies have analyzed their organic chemistry and molecular parameters, suggesting that the source of the bituminous limestones contains a mixture of aquatic (algal and bacterial) and terrigenous organic matter (Kara-Gülbay et al. 2012).

The studied limestone samples exhibit characteristics of low Mg-calcite with the chemical formula of $Ca_{98.81–99.52}Mg_{0.48–1.19}(CO_3)$. Low-Mg calcite is considered to be more stable relative to High-Mg calcitic and aragonitic components (e.g., Hashim and Kaczmarek 2020). The $\delta^{13}C$ values (− 2.19 to − 0.90, − 1.40‰) slightly overlap with the measured $\delta^{13}C$ values of the Aptian carbonate and foraminifera (0 to 4.0 ‰, Veizer et al. 1999; Huck et al., 2011). The $\delta^{18}O$ data (− 4.90 to − 3.53 with ave. −4.50) are slightly lower than those of belemnite fossils (− 3.49 to − 1.75, with an average of − 2.75; Özyurt et al. 2022), which implies diagenetic influence or freshwater involvements or high T. They have low Mn/Sr ratios of less than 3, confirming a high degree of preservation of primary geochemical signatures (Veizer and Hoefs 1976). They are mainly represented by a (1) low REE content (mean 12.80 ppm), (2) LREE depletion relative to the HREEs (ave. 0.62 of La/Yb_N and mean 0.54 of Nd/Yb_N), (3) positive La anomaly (ave. 2.82 of La*/La) and (4) chondritic Y/Ho (29.17–50.00, with an average 35). The REE chemistry of the LBL facies well conforms with marine sediments. However, their Sr (499–879 with ave. 701 ppm) contents are strongly higher than carbonates formed in normal seawater (Sr $\approx$ 250 ppm; Tucker and Wright 2009; Swart et al. 2005). Their Sr contents overlap with seawater with very high salinities derived from the hypersaline sabkhas ($\approx$550 ppm; Tucker and Wright 2009). Thus, diagnostic seawater signature with high Sr reflects an isolated basin that was transformed from a marine to a lagoon setting. Besides, the low Mo/TOC (0.70–3.69; ave. 2.41) supports a certain degree of water restriction (Algeo and Rowe 2012).

On the other hand, the geochemical characteristics of carbonates have been widely used as an important proxy for constraining the tectonic setting of sedimentary basins (Bau 1996; Nothdurft et al. 2004; Zhang et al. 2017; Satish-Kumar et al. 2021). A recent review by Zhang et al. (2017) focused on the chemistry of a wide range of limestones deposited in various plate tectonic settings. In this contribution, the researchers proposed that the geochemical traces can be successfully applied to differentiate the carbonates accumulated in passive and active continental margins, oceanic highs and islands in open oceans, and inland basins. They suggested that REE patterns such as La/Sm_N, Sm/Yb_N, Eu/Eu*, and Ce/Ce* values that are combined with immobile elements (i.e. Zr, Ti, La, and Sc) can provide a better understanding of the depositional setting of carbonate rocks. It is also noted that the inland carbonates are highlighted by relatively elevated Eu/Eu* values (average 3.74). The studied samples display relatively lower Eu/Eu* ratios (1.23–1.53 with an average of 1.35) compared to inland carbonates. However, they are mostly plotted in the field of inland and margin carbonates (Fig. 5f–g). Their Zr/Ti values are higher than margin carbonates and they are mostly compatible with inland carbonates. Hence, REE chemical evidence confirms a deposition of the LBL in an inland environment.

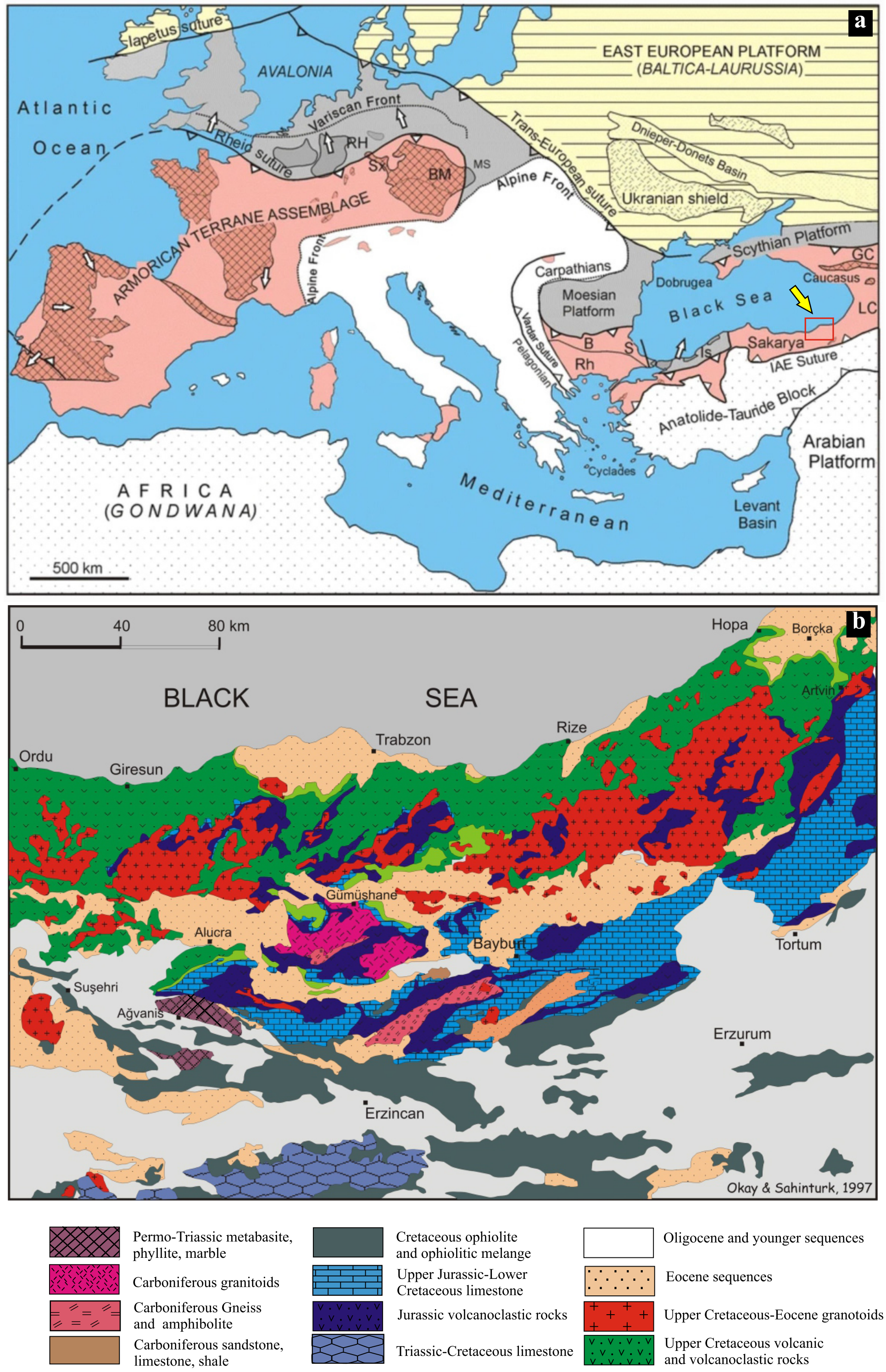

Fig. 1 **a** A global tectonic map displaying the main tectonic units in Europe and the Black Sea region. B Balkanides, BM Bohemian Massif, Is Istanbul Zone, GC Greater Caucasus, IAE Izmir–Ankara–Erzincan, LC Lesser Caucasus, Ms. Moravia–Silesia, Rh Rhodope Massif, RH Rheno-Hercynian, St Strandja Massif (Okay and Topuz 2017). **b** Generalized geologic map of Eastern Pontides, Eastern Black Sea region (modified Okay and Şahintürk 1997)

4.3 Redox conditions

The redox-sensitive trace elements (RSE) such as Fe, Mn, Mo, Cu, Ni, and Zn have been widely used as a potential proxy for the redox status of depositional setting (Tribovillard et al. 2006; Scott et al. 2008; Sahoo et al. 2012; Miller et al. 2017). These elements tend to form soluble oxyanions under oxic conditions whereas become less soluble under oxygen deficiency conditions (e.g., Bruland and Lohan 2006). This causes RSE enrichments in sedimentary basins with oxygen-depleted conditions (Scott et al. 2008; Sahoo et al. 2012; Miller et al. 2017). The Mn

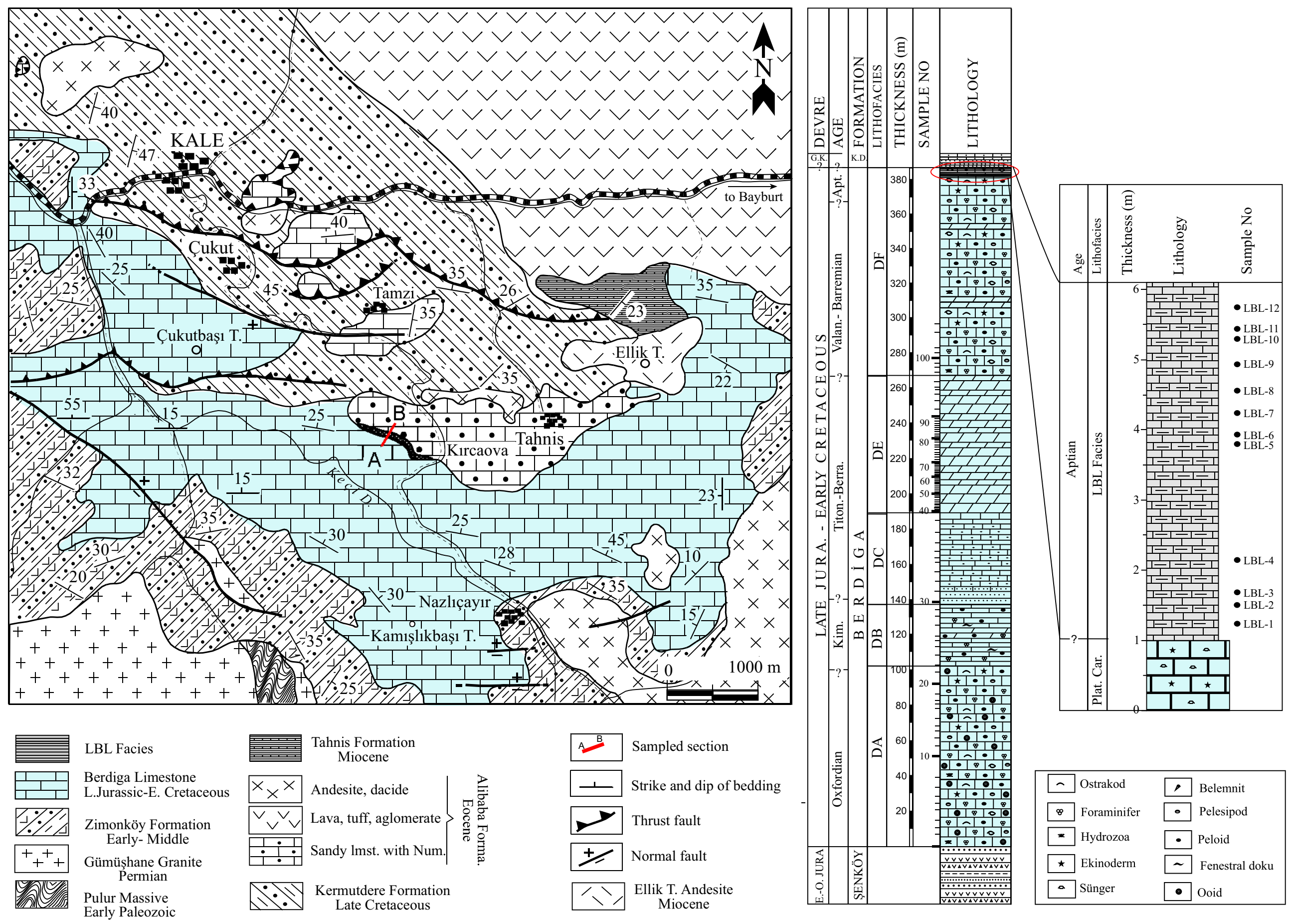

Fig. 2 Geological map of the Kırcaova (Gümüşhane) area (modified from Kırmacı et al. 1996). Insets displaying the general lithofacies distribution in the Berdiga Fm (Kırmacı et al. 1996). The black ellipsis shows LBL strata. The stratigraphic section of LBL strata

and Fe contents of the studied samples are relatively higher than marine sediments (vary from 3 to 50 ppm; Veizer 2018), implying an increase in Mn and Fe contents or reducing conditions (Brand and Veizer 1980; Swart et al.2015). Their Mo, Cu, Zn, and Ni contents are higher than those of marine setting (Table 2; Özyurt in prep.). The other important indicator of oxygenated conditions can be considered a pronounced negative Ce/Ce* anomaly (Nozaki 2001; Shields and Webb 2004; Bau et al. 2010). The studied LBL samples display a lack of significant negative-Ce anomalies implying low oxygenated conditions (e.g., Özyurt et al. 2020). Their Pr/Ph values (Apr. 1.3; Kara-Gülbay et al. 2012) further confirm the oxygen-depleted conditions.

4.4 Paleoclimate conditions

Paleoclimatic conditions play an important role in water chemistry, organism types, paleosalinity, and pH of the lacustrine basin (Rohais et al. 2019; Wu et al. 2021; Kong et al. 2022). Sr/Cu has been widely used as a paleoclimate indicator (Wang et al. 2018a, b; Xu et al. 2021). According to Lerman and Wang (1989), Sr/Cu ratios that are lower than 5.0 imply a warm-humid climate, whereas ratios higher than 5.0 indicate a warm-humid climate. Later, Jia et al. (2013) argue against the borderline, because Sr and Cu contents can be influenced by the basin geomorphology such as scale and water depth for lacustrine sediment. They have proposed that the Sr/Cu ratio lower than 10 implies a warm and moist climate, but Sr/Cu ratio higher than 10 suggests a hot and arid climate. The studied LBL samples possess strongly high Sr/Cu ratios (ave. 402.06) which mostly show hot and arid climate conditions. In addition, Sr and Ba are alkaline-Earth metals that display different geochemical fractionation in a sedimentary environment. Sr/Ba can be used as important paleoclimate parameters (Meng et al. 2012). The Sr/Ba ratios much less than 0.5 indicate low salinity seawater on the shelf with unrestricted marine environmental conditions and less water evaporation. The high Sr/Ba values are used as indicators of high salinity environmental conditions or hot arid paleoclimatic conditions climate, whereas a low Sr/Ba value represents

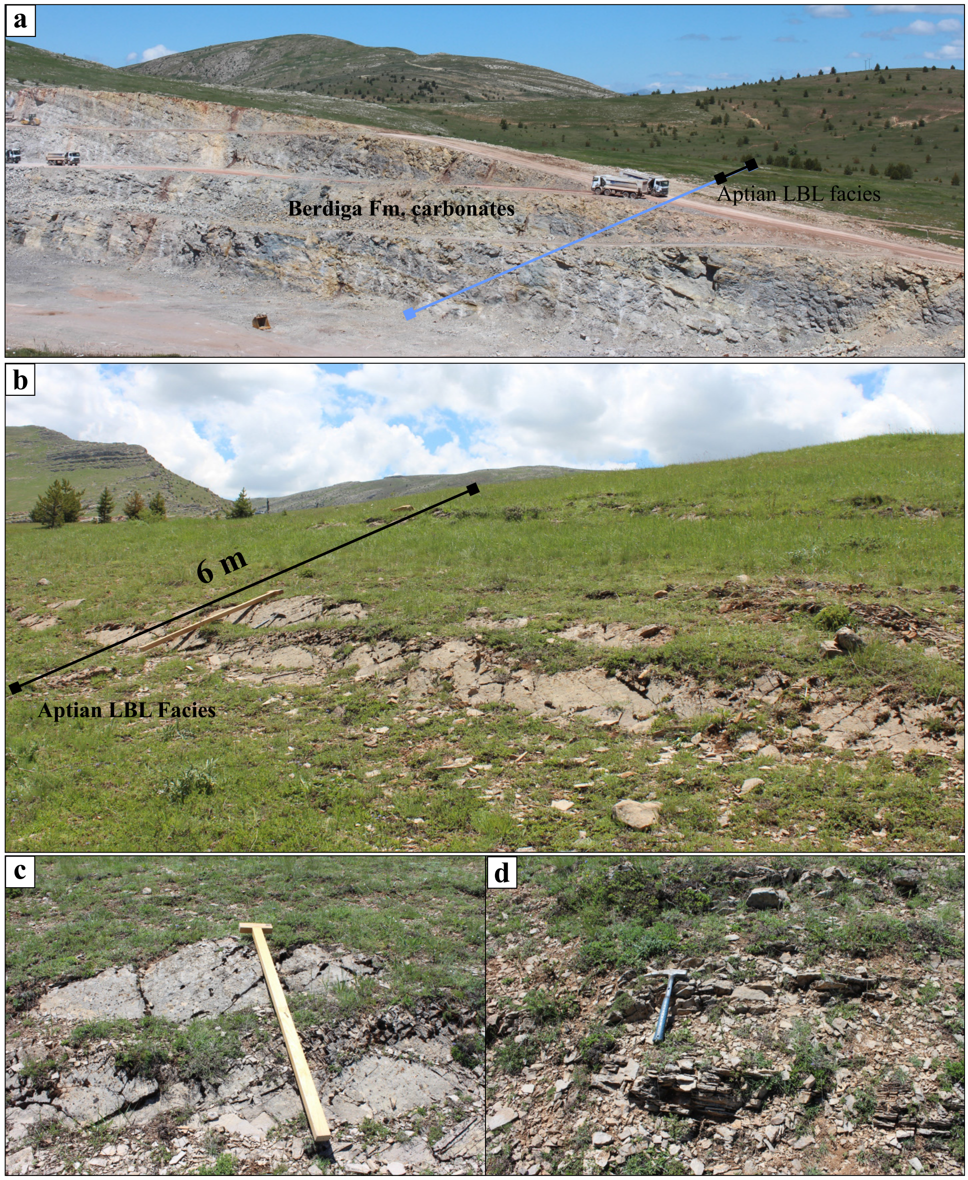

Fig. 3 **a** Geological field view of Berdiga Fm. and LBL strata, **b** general view of the approximately 6 m thick, dark grey LBL strata, **c** the lower part of thin to medium bedded limestone facies, and **d** upper part of the laminated LBL strata

Table 2 Redox sensitive elements (RSE) and correlation with Berdiga Fm

	LBL samples										Inner Platform Carbonates (Özyurt et al. 2020)	
	LBL-1	LBL-2	LBL-3	LBL-4	LBL-5	LBL-6	LBL-7	min	max	ave	Min	Max
Co	0.50	0.50	0.20	0.50	2.20	1.80	2.20	0.20	2.20	1.13	0.40	0.70
Mo	0.70	1.50	1.20	0.30	4.10	4.20	2.60	0.30	4.20	2.09	0.20	0.40
Cu	1.20	1.20	1.40	0.80	4.90	3.50	5.80	0.80	5.80	2.69	0.40	0.90
Zn	2.00	3.00	3.00	1.00	7.00	6.00	12.00	1.00	12.00	4.86	2.00	7.00
Ni	2.80	4.20	4.10	0.90	7.60	4.40	7.80	0.90	7.80	4.54	1.80	2.00

low salinity or warm humid climate. The LBL samples display high Sr/Ba (40.26–78.47; ave. 52.74), confirming Cretaceous conditions. Despite the high Sr, Sr/Cu, and Sr/Ba of the studied LBL samples suggesting extreme hot-house and dry climatic conditions, no syn-sedimentary dolomite or evaporites are observed in the studied

Fig. 4 Microfacies microphotographs of GBL strata (**a**–**d**). **a** Wackestone–mudstone with allochthonous bioclasts including ostracod and characean stems, **b** Wackestone with gastropods, **c**, **d** Wackestone-mudstone LBL strata with ostracod and gastropods. Ch: characean, G: gastropods

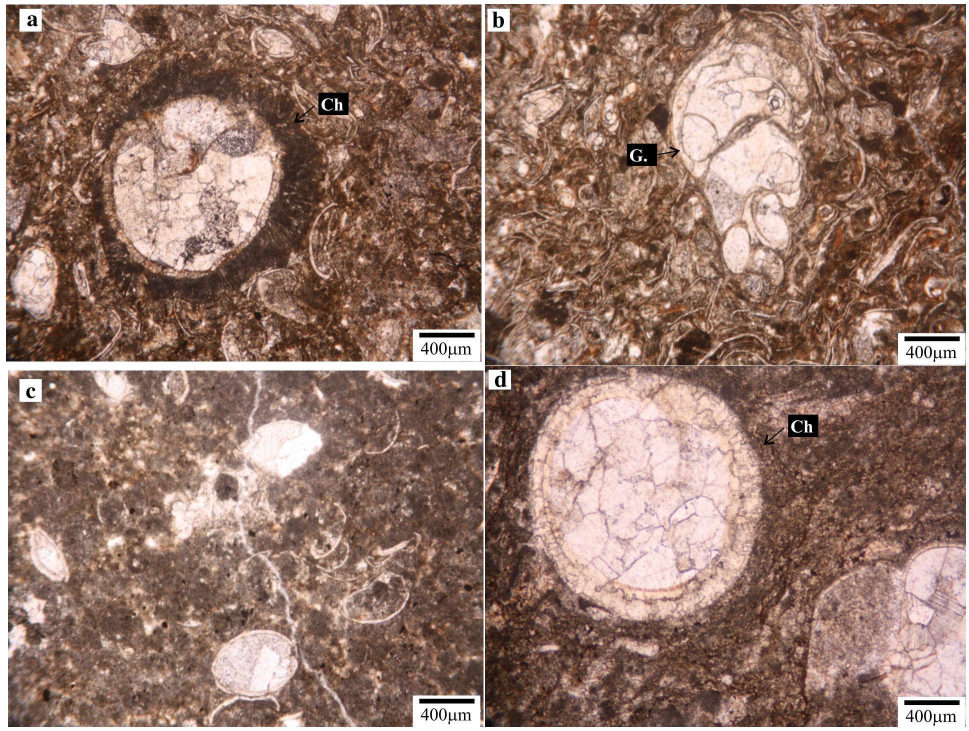

section. The extremely high values of Sr-depended indicators can be related to their carbonate dominant lithology, because Ca and Sr display similar electronegativities, ionic radii, and ionization character, and Sr tends to be incorporated in carbonate minerals.

On the other hand, Ga and Al have a close association with the fine-grained aluminosilicate fraction, and these elements are commonly enriched in kaolinite linked to warm and humid and warm climate conditions (e.g., Hieronymus et al. 2001; Roy and Roser 2013). Rb and P are linked to illite, which implies low chemical weathering under cold and dry climatic conditions (e.g., Ratcliffe et al. 2010). Thus, their relative enrichment has been widely used as weathering and paleoclimatic indicators (Beckmann et al. 2005; Xu et al. 2022). The studied samples have low Ga/Rb (0.16–0.50; an average of 0.31) and high K/Al ratios (0.12–0.16; an average of 0.14) might indicate a trend into hot and semi-humid conditions. Our results are broadly consistent with published data from the Aptian strata and with estimates for mid-Cretaceous latitudinal gradients (Larson and Erba 1999; Leckie et al. 2002; Jenkyns 2010; Föllmi 2012; Lechler et al. 2015; Navarro-Ramirez et al. 2017).

4.5 Organic matter enrichment

The LBL horizons consist of thin, bituminous decimetre-thick sequences (e.g., Kırmacı et al. 1996; Kirmaci et al. 1996). They are well correlated with Aptian bitumen limestone in the other Tethys Reams of N Germany, Slovenia, Greece, and Türkiye (Koch and Zimmerle 1996). These horizons are considered episodes of increased organic matter (Koch and Zimmerle 1996; Kara-Gülbay et al. 2012). The microfacies, fossil assemblage, and REEs of the studied LBL samples suggest an isolated basin with high alkalinity and nutrient levels. Although, the basin periodically can be supplied by fresh water through run-off or river. The studied rocks display low Zr, and Hf contents which support input of rainwater instead of river flux that can release considerably high amounts of REE, Zr, Hf, and Sc. The high Sr, Na, Sr/Cu, K/Al, and low Ga/Rb suggest extreme hothouse climatic conditions.

During an extremely hothouse climatic event, evaporation increased, leading to the high concentration of the isolated basin and a sudden rise in paleosalinity. Subsequently, the hot and semi-arid palaeoclimate weakened slightly, and gradually increasing run-off resulted in a period of high rainfall (Luz 1979; Pratt 1984). In this context, the run-off cycle had a strong influence on the periodic freshwater supply to the environment, in which characian fossils enriched in the surface water (Kırmacı et al. 1996; Kara-Gülbay et al. 2012). This also raised nutrient levels in the environment, resulting in high productivity (Jenkyns 1999; Leckie et al. 2002; Erba 2004). Freshwater formed lighter water above the denser saline water below (Luz 1979; Pratt 1984; Waples 2013). The oxygen could not be introduced to the lower water layer where the LBL sedimentation was occurring. The

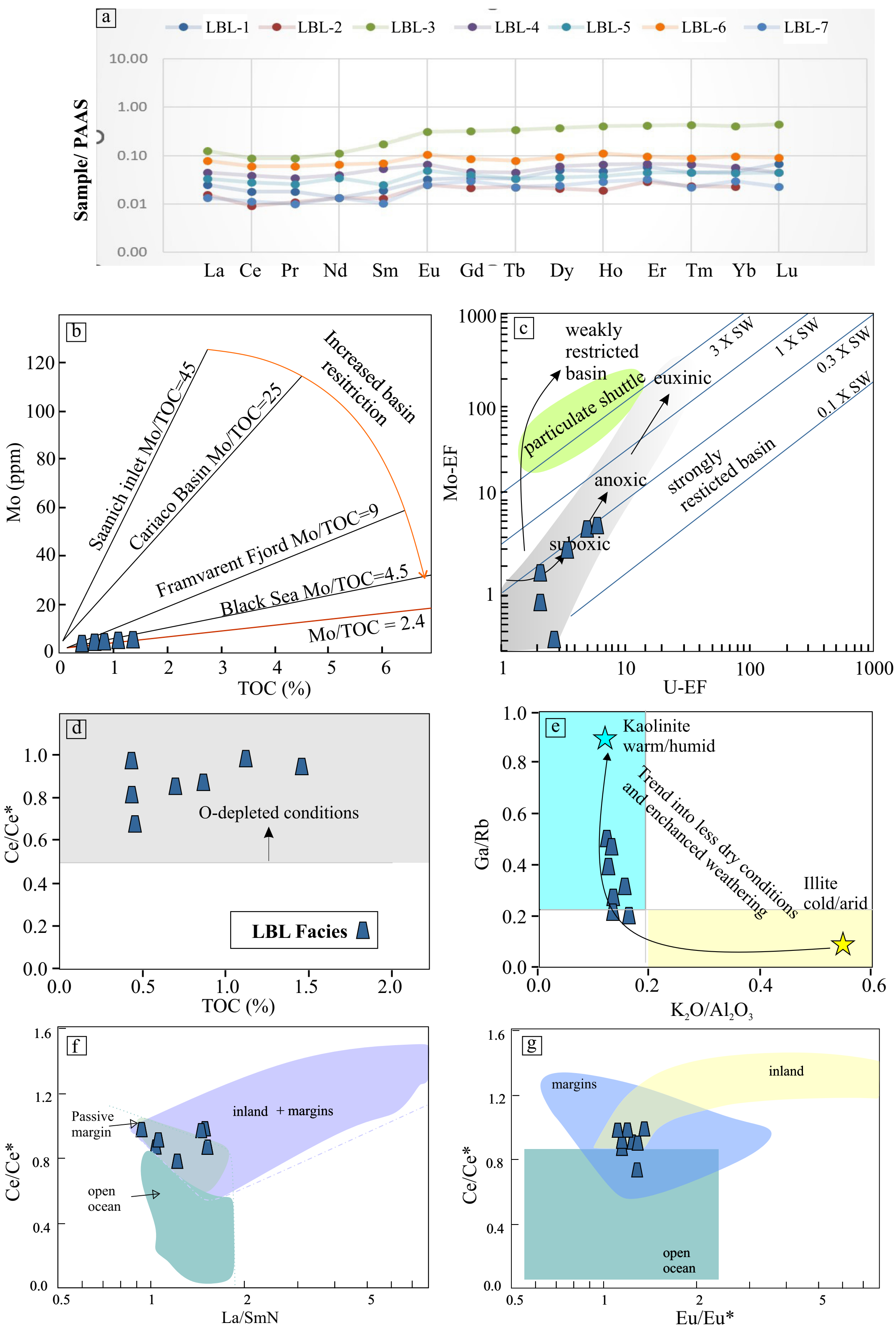

Fig. 5 **a** Plots of the PAAS normalized data PAAS-normalized REE patterns of the studied LBL strata; **b** TOC vs Mo; **c** U_{EF} vs Mo_{EF}; **d** TOC vs Ce/Ce*; **e** K_2O/Al_2O_3 vs Ga/Rb; **f** La/Sm_N vs Ce/Ce* and **g** Eu/Eu* vs Ce/Ce*. The fields of passive margin, open ocean, and inland basin are taken from the study by Zhang et al. (2017). The fields of warm/humid and cold/arid climate conditions are adapted from the study by Roy and Roser, 2013

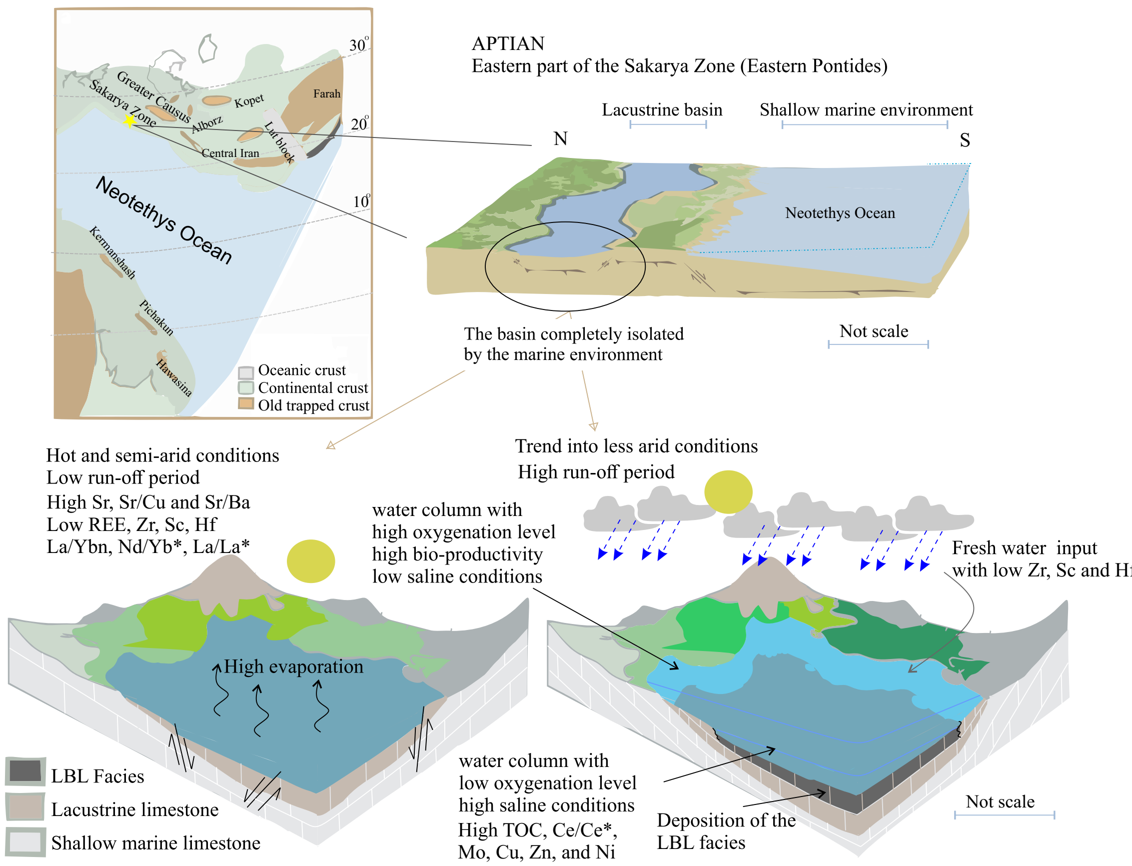

Fig. 6 **a** The paleogeographic map displays the Aptian evolution the of Neotethys Ocean (modified from Karslı et al. 2021). Star mark study area. **b** Diagrammatic sketches illustrate a conceptual model for paleogeography and paleoclimate factors controlling the organic matter enrichment. The marine environment was transformed into a lagoon environment with a lack of marine influence or possible lacustrine setting. The geochemistry of the LBL records of the Aptian hot house climate conditions with periodic change. In this context, the run-off cycle had a strong influence on the periodic freshwater supply to the environment, in which characian fossils enriched in the surface water. This also raised nutrient levels in the environment, resulting in high bio-productivity. The period of high rainfall resulted in a freshwater supply with low salinity to the depositional environment, leading to water column stratifications. High-salinity stratified water columns occurred in the bottom water with suboxic to relatively anoxic conditions. This led to a high preservation rate of TOC at the bottom

difference in chemistry between fresh water and saline fluids with higher density also led to water stratifications (Arthur and Natland 1979). This was probably followed by steady stratification, which results in the anoxic bottom water, increasing the preservation potential of organic matter (Wang et al. 2018a, b). Meanwhile, the oxygen content of bottom water decreased, which resulted in the enrichment of RSE, Ce/Ce* values, and TOC values (Fig. 6).

Overall, a greenhouse climate was accompanied by high primary productivity. The combination of these sedimentary processes favored the deposition of organic-rich limestone in the lacustrine settings of the Eastern Black Sea Region (Fig. 6). Our results are conformable with the published data from marine (e.g., Jenkyns 2010; Heimhofer et al. 2004; Quijano et al. 2012; Bottini et al. 2015; Basilone 2021; Fang et al. 2021), semi-restricted basin (e.g., Sanchez-Hernandez and Florentin 2016; Socorro et al. 2017; Socorro and Maurrasse 2019) and lacustrine settings (e.g., Zhang et al. 2020; Deconinck et al. 2021) in the different parts of the Tethys margin.

5 Conclusion

The sedimentological and geochemical analyses of the Aptian LBL facies allow us to reconstruct sedimentary conditions as outlined in Fig. 6.

Our primary results are as follows:

1. The LBL facies were deposited in the isolated basin with oxygen-depleted conditions.
2. The LBL facies record hot and semi-arid to semi-humid climate conditions. The periodic change in paleoclimate causes enhanced weathering, resulting in a high run-off and freshwater supply. The weathering processes lead to the nutrient flux into the depositional

environment through time. This increases bio-productivity within the shallow zone of the water columns, as supported by relatively high TOC content.

3. The water column exhibits high salinity and is suboxic to relatively anoxic conditions at the bottom. These bottom water conditions contribute to the preservation of organic matter during sedimentation.
4. The regional parameters such as the climate, increased run-off period, nutrient levels, alkalinity level, and dominant carbonate producers (algal organisms and other saprofer) favored the enrichment in organic-rich facies during the Aptian.
5. Extreme Cretaceous conditions are important factors controlling organic matter enrichment. Our results are conformable with the published data in the different parts of the Tethys margin. Therefore, this approach may provide the first insight into the paleo-climate conditions for the Eastern Black Sea (NE Turkey).

Acknowledgements The corresponding author acknowledges the Karadeniz Technical University for facilitating her research and for access to the Sedimentary Laboratories during the micro-drilling sampling period. The author is grateful to Prof. Dr. Ihsan Al-Aasm (University of Windsor, Canada) for the stable isotope ($\delta^{18}O$ and $\delta^{13}C$) analyses. The appreciation is extended to Prof. Dr. Cathy Hollis (University of Manchester, UK) for her supervision during the author's Post-Doc Research focusing on REE chemistry of carbonates. The appreciation is extended to Prof. Dr. Reyhan Kara Gülbay (Karadeniz Technical University, Türkiye) and M. Ziya Kırmacı (Karadeniz Technical University, Türkiye) for their constructive comments, which greatly improved the quality of this paper. Thanks also due to Ali Keskin and Aslı Çağla for their help during the field and laboratory studies.

Funding This research did not receive any specific grant from funding agencies in the public, commercial, or not-for-profit sectors.

Declarations

Conflict of interest The author declares that they have no known competing financial interests or personal relationships that could have appeared to influence the work reported in this paper.

References

Akdoğan R, Okay AI, Dunkl I (2018) Triassic-Jurassic arc magmatism in the Pontides as revealed by the U-Pb detrital zircon ages in the Jurassic sandstones of northeastern Turkey. Turkish J Earth Sci 27(2):89–109

Algeo TJ, Rowe H (2012) Paleoceanographic applications of trace-metal concentration data. Chem Geol 324:6–18

Arslan M, Aliyazicioglu I (2001) Geochemical and petrological characteristics of the Kale (Gümüshane) volcanic rocks: implications for the Eocene evolution of eastern Pontide arc volcanism, northeast Turkey. Int Geol Rev 43(7):595–610

Arthur MA, Natland JH (1979) Carbonaceous sediments in the North and South Atlantic: The role of salinity in stable stratification of Early Cretaceous basins. Deep Drilling Results in the Atlantic Ocean: Continental Margins and Paleoenvironment 3:375–401

Arthur MA, Sageman BB (1994) Marine black shales: depositional mechanisms and environments of ancient deposits. Annu Rev Earth Planet Sci 22(1):499–551

Banner JL, Hanson GN, Meyers WJ (1988)Rare earth element and Nd isotopic variations in regionally extensive dolomites from the Burlington-Keokuk Formation (Mississippian); implications for REE mobility during carbonate diagenesis. Journal of Sedimentary Research, 58(3):415–432.

Basilone L (2021) Synsedimentary tectonics vs paleoclimatic changes across the Aptian-Albian boundary along the Southern Tethyan margin: The panormide carbonate platform case history (NW Sicily). Mar Pet Geol 124:104801

Bau M (1991) Rare-earth element mobility during hydrothermal and metamorphic fluid-rock interaction and the significance of the oxidation state of europium. Chem Geol 93(3–4):219–230

Bau M (1996) Controls on the fractionation of isovalent trace elements in magmatic and aqueous systems: evidence from Y/Ho, Zr/Hf, and lanthanide tetrad effect. Contrib Miner Petrol 123(3):323–333

Bau M, Dulski P (1996) Distribution of yttrium and rare-earth elements in the Penge and Kuruman iron-formations, Transvaal Supergroup. South Africa Precambrian Res 79(1–2):37–55

Bau M, Balan S, Schmidt K, Koschinsky A (2010) Rare earth elements in mussel shells of the Mytilidae family as tracers for hidden and fossil high-temperature hydrothermal systems. Earth Planet Sci Lett 299(3–4):310–316

Beckman B, Wagner T, Hofmann P (2005) Linking Coniacian–Santonian (OAE3) black-shale deposition to African climate variability: A reference section from the eastern tropical Atlantic at orbital time scales (ODP Site 959, off Ivory Coast and Ghana).

Bottini C, Erba E, Tiraboschi D, Jenkyns HC, Schouten S, Sinninghe Damsté JS (2015) Climate variability and ocean fertility during the Aptian Stage. Clim Past 11(3):383–402

Boynton WV (1984) Cosmochemistry of the rare earth elements: meteorite studies. In: Developments in geochemistry, vol. 2, pp. 63–114. Elsevier, Amsterdam.

Brand U, Veizer J (1980) Chemical diagenesis of a multicomponent carbonate system; 1, Trace elements. J Sediment Res 50(4):1219–1236

Bruland KW, Lohan MC (2006) Controls of trace metals in seawater. Oceans Mar Geochem 6:23–47

Burdige DJ (2007) Preservation of organic matter in marine sediments: controls, mechanisms, and an imbalance in sediment organic carbon budgets? Chem Rev 107(2):467–485

Byrne RH, Sholkovitz ER (1996) Marine chemistry and geochemistry of the lanthanides. Handb Phys Chem Rare Earths 23:497–593

De Baar HJ (1991) On cerium anomalies in the Sargasso Sea. Geochim Cosmochim Acta 55(10):2981–2983

Deconinck JF, Boué D, Amédro F, Baudin F, Bruneau L, Huret E, Landrein P, Moreau J-D, Santoni AL (2021) First record of early Aptian Oceanic Anoxic Event 1a from the Paris Basin (France)-Climate signals on a terrigenous shelf. Cretac Res 125:104846

Demaison GJ, Moore GT (1980) Anoxic environments and oil source bed genesis. AAPG Bull 64(8):1179–1209

Dokuz A, Tanyolu E (2006) Geochemical constraints on the provenance, mineral sorting and subaerial weathering of Lower Jurassic and Upper Cretaceous clastic rocks of the eastern Pontides, Yusufeli (Artvin), NE Turkey. Turkish J Earth Sci 15(2):181–209

Dokuz A, Karsli O, Chen B, Uysal İ (2010) Sources and petrogenesis of Jurassic granitoids in the Yusufeli area, Northeastern Turkey: implications for pre-and post-collisional lithospheric thinning of the eastern Pontides. Tectonophysics 480(1–4):259–279

Dunham RJ (1962) Classification of carbonate rocks according to depositional textures. Amer. Assoc. Petroleum Geologists, Memoir No. 1, pp 108–121.

Elderfield H (1988) The oceanic chemistry of the rare-earth elements. Philos Trans Roy Soc Lond Series A Math Phys Sci 325(1583):105–126.

Erba E (2004) Calcareous nannofossils and Mesozoic oceanic anoxic events. Mar Micropaleontol 52(1–4):85–106

Eren M, Tasli K (2002) Kilop cretaceous hardground (Kale, Gümüshane, NE Turkey): description and origin. J Asian Earth Sci 20(5):433–448

Eyuboglu Y, Santosh M, Dudas FO, Akaryalı E, Chung SL, Akdağ K, Bektaş O (2013) The nature of transition from adakitic to non-adakitic magmatism in a slab window setting: a synthesis from the eastern Pontides. NE Turkey Geosci Front 4(4):353–375

Fang P, Luo H, Xu B, Huber BT, Zhu Y, Mu L (2021) Planktic foraminifera of the upper Barremian-Aptian black shale intervals from the Chaqiela section (Gamba, southern Tibet): Biostratigraphic and palaeoenvironmental implications. Cretac Res 127:104934

Flügel E (2012) Microfacies analysis of limestones. Springer, Cham

Föllmi KB (2012) Early Cretaceous life, climate and anoxia. Cretac Res 35:230–257

Franchi F (2018) Petrographic and geochemical characterization of the Lower Transvaal Supergroup stromatolitic dolostones (Kanye Basin, Botswana). Precambr Res 310:93–113

Frimmel HE (2009) Trace element distribution in Neoproterozoic carbonates as palaeoenvironmental indicator. Chem Geol 258(3–4):338–353

German CR, Elderfield H (1989) Rare earth elements in Saanich Inlet, British Columbia, a seasonally anoxic basin. Geochim Cosmochim Acta 53(10):2561–2571

German CR, Elderfield H (1990) Application of the Ce anomaly as a paleoredox indicator: the ground rules. Paleoceanography, 5(5), 823-833.

Gong Q, Li F, Lu C, Wang H, Tang H (2021) Tracing seawater-and terrestrial-sourced REE signatures in detritally contaminated, diagenetically altered carbonate rocks. Chem Geol 570:120169

Görür N (1988) Timing of opening of the Black Sea basin. Tectonophysics 147(3–4):247–262

Hashim MS, Kaczmarek SE (2020) Experimental stabilization of carbonate sediments to calcite: insights into the depositional and diagenetic controls on calcite microcrystal texture. Earth Planet Sci Lett 538:116235

Heimhofer U, Hochuli PA, Herrle JO, Andersen N, Weissert H (2004) Absence of major vegetation and palaeoatmospheric pCO2 changes associated with oceanic anoxic event 1a (Early Aptian, SE France). Earth Planet Sci Lett 223(3–4):303–318

Hieronymus B, Kotschoubey B, Boulègue J (2001) Gallium behaviour in some contrasting lateritic profiles from Cameroon and Brazil. J Geochem Explor 72(2):147–163

Huck S, Heimhofer U, Rameil N, Bodin S, Immenhauser A (2011) Strontium and carbon-isotope chronostratigraphy of Barremian-Aptian shoal-water carbonates: Northern Tethyan platform drowning predates OAE 1a. Earth Planet Sci Lett 304(3–4):547–558

Jenkyns HC (2010) Geochemistry of oceanic anoxic events. Geochem Geophys Geosyst 11(3).

Jenkyns HC (1999) Mesozoic anoxic events and palaeoclimate. Zbl Geol Paläontol 1997(7–9):943–949

Jia J, Liu Z, Bechtel A, Strobl SA, Sun P (2013) Tectonic and climate control of oil shale deposition in the Upper Cretaceous Qingshankou Formation (Songliao Basin, NE China). Int J Earth Sci 102:1717–1734

Kandemir R, Yılmaz C (2009) Lithostratigraphy, facies, and deposition environment of the lower Jurassic Ammonitico Rosso type sediments (ARTS) in the Gümüşhane area, NE Turkey: implications for the opening of the northern branch of the Neo-Tethys Ocean. J Asian Earth Sci 34(4):586–598

Kandemir R, Özyurt M, Karsli O (2022) Sedimentological and geochemical characteristics of Lower Jurassic Sandstones from Gümüşhane, NE Turkey: implications for source to sink processes, paleoenvironmental conditions, provenance and tectonic settings. Int Geol Rev 64(12):1719–1742

Kara-Gülbay R, Kırmacı MZ, Korkmaz S (2012) Organic geochemistry and depositional environment of the Aptian bituminous limestone in the Kale Gümüşhane area (NE-Turkey): an example of lacustrine deposits on the platform carbonate sequence. Org Geochem 49:6–17

Karsli O, Dokuz A, Uysal I, Aydin F, Chen B, Kandemir R, Wijbrans J (2010) Relative contributions of crust and mantle to generation of Campanian high-K calc-alkaline I-type granitoids in a subduction setting, with special reference to the Harşit Pluton, Eastern Turkey. Contrib Miner Petrol 160:467–487

Karsli O, Ilhan M, Kandemir R, Dokuz A, Aydin F, Uysal İ, Duygu L (2021) Nature of the Early Cretaceous lamprophyre and high-Nb basaltic dykes, NE Turkey: constraints on their linkage to subduction initiation of Neotethyan oceanic lithosphere. Lithos 380:105884

Kaygusuz A, Aydınçakır E (2009) Mineralogy, whole-rock and Sr–Nd isotope geochemistry of mafic microgranular enclaves in Cretaceous Dagbasi granitoids, Eastern Pontides, NE Turkey: evidence of magma mixing, mingling and chemical equilibration. Geochemistry 69(3):247–277

Kaygusuz A, Arslan M, Siebel W, Sipahi F, Ilbeyli N (2012) Geochronological evidence and tectonic significance of Carboniferous magmatism in the southwest Trabzon area, eastern Pontides. Turkey Int Geol Rev 54(15):1776–1800

Kaygusuz A, Chen B, Aslan Z, Siebel W, Şen C (2009) U-Pb zircon SHRIMP ages, geochemical and Sr-Nd isotopic compositions of the Early Cretaceous I-type Sarıosman pluton, Eastern Pontides, NE Turkey. Turkish J Earth Sci 18(4):549–581

Kirmaci MZ, Koch R, Bucur JI (1996) An Early Cretaceous section in the Kircaova Area (Berdiga Limestone, NE-Turkey) and its correlation with platform carbonates in W-Slovenia. Facies 34(1):1–21

Kırmacı MZ, Yıldız M, Kandemir R, Eroğlu-Gümrük T (2018) Multistage dolomitization in Late Jurassic-Early Cretaceous platform carbonates (Berdiga Formation), Başoba Yayla (Trabzon), NE Turkey: Implications of the generation of magmatic arc on dolomitization. Mar Pet Geol 89:515–529

Koch R, Bucur II, Kirmaci MZ, Eren M, Tasli K (2008) Upper Jurassic and lower Cretaceous carbonate rocks of the Berdiga Limestone–Sedimentation on an onbound platform with volcanic and episodic siliciclastic influx. Biostratigraphy, facies and. Neues Jahrbuch fur Geologie und Palaontologie-Abhandlungen 247(1):23–62.

Koch R, Zimmerle W (1996) Sedimentological–geochemical and biostratigraphic correlation of Aptian/Albian black shales (N-Germany–Slovenia–Greece–Turkey). Global and regional controls on biogenic sedimentation. II. Cretaceous sedimentation. Research Reports.-Göttinger Arb. Geol. Paläont., Sb, 3, 51–59.

Koeppenkastrop D, Eric H (1992) Sorption of rare-earth elements from seawater onto synthetic mineral particles: an experimental approach. Chem Geol 95(3–4):251–263

Kong X, Jiang Z, Ju B (2022) Hydrocarbon accumulation characteristics in the inter-salt shale oil reservoir in the Eocene Qianjiang Depression, Hubei Province, China. J Petrol Sci Eng 211:110117

Larson RL, Erba E (1999) Onset of the Mid-Cretaceous greenhouse in the Barremian-Aptian: Igneous events and the biological, sedimentary, and geochemical responses. Paleoceanography 14(6):663–678

Lechler M, von Strandmann PAP, Jenkyns HC, Prosser G, Parente M (2015) Lithium-isotope evidence for enhanced silicate weathering during OAE 1a (Early Aptian Selli event). Earth Planet Sci Lett 432:210–222

Leckie RM, Bralower TJ, Cashman R (2002) Oceanic anoxic events and plankton evolution: Biotic response to tectonic forcing during the mid-Cretaceous. Paleoceanography 17(3):13–21

Lerman A, Wang SM (1989) Translated, Lakes-Chemistry Geology Physics.

Li F, Yan J, Burne RV, Chen ZQ, Algeo TJ, Zhang W, Tian L, Gan Y, Liu K, Xie S (2017) Paleo-seawater REE compositions and microbial signatures preserved in laminae of Lower Triassic ooids. Palaeogeogr Palaeoclimatol Palaeoecol 486:96–107

Liu XM, Hardisty DS, Lyons TW, Swart PK (2019) Evaluating the fidelity of the cerium paleoredox tracer during variable carbonate diagenesis on the Great Bahamas Bank. Geochim Cosmochim Acta 248:25–42

Luz B (1979) Palaeo-oceanography of the post-glacial eastern Mediterranean. Nature 278:847–848

Meng Q, Liu Z, Bruch AA, Liu R, Hu F (2012) Palaeoclimatic evolution during Eocene and its influence on oil shale mineralisation, Fushun basin, China. J Asian Earth Sci 45:95–105

Miller AJ, Strauss JV, Halverson GP, Macdonald FA, Johnston DT, Sperling EA (2017) Tracking the onset of Phanerozoic-style redox-sensitive trace metal enrichments: new results from basal Ediacaran post-glacial strata in NW Canada. Chem Geol 457:24–37

Mort H, Jacquat O, Adatte T, Steinmann P, Föllmi K, Matera V, Berner Z, Stüben D (2007) The Cenomanian/Turonian anoxic event at the Bonarelli Level in Italy and Spain: enhanced productivity and/or better preservation? Cretac Res 28(4):597–612

Murphy AE, Sageman BB, Hollander DJ (2000) Eutrophication by decoupling of the marine biogeochemical cycles of C, N, and P: a mechanism for the Late Devonian mass extinction. Geology 28(5):427–430

Navarro-Ramirez JP, Bodin S, Consorti L, Immenhauser A (2017) Response of western South American epeiric-neritic ecosystem to middle Cretaceous Oceanic Anoxic Events. Cretac Res 75:61–80

Nothdurft LD, Webb GE, Kamber BS (2004) Rare earth element geochemistry of Late Devonian reefal carbonates, Canning Basin, Western Australia: confirmation of a seawater REE proxy in ancient limestones. Geochim Cosmochim Acta 68(2):263–283

Nozaki Y (2001) Rare earth elements and their isotopes in the ocean. Encyclopedia Ocean Sci 4:2354–2366

Okay AI, Nikishin AM (2015) Tectonic evolution of the southern margin of Laurasia in the Black Sea region. Int Geol Rev 57(5–8):1051–1076

Okay AI, Sahinturk O (1997) AAPG Memoir 68: Regional and Petroleum Geology of the Black Sea and Surrounding Region. Chapter 15: Geology of the Eastern Pontides.

Okay AI, Topuz G (2017) Variscan orogeny in the Black Sea region. Int J Earth Sci 106:569–592

Özyurt M (2019) Origin of Dolomitization in Upper Jurassıc-Lower Cretaceous Platform Carbonates (Berdiga Formatıon) in Gümüşhane Area, PhD Thesis, Karadeniz Technical University, Turkey.

Özyurt M, Kırmacı MZ, Al-Aasm IS (2019a) Geochemical characteristics of Upper Jurassic-Lower Cretaceous platform carbonates in Hazine Mağara, Gümüşhane (northeast Turkey): implications for dolomitization and recrystallization. Can J Earth Sci 56(3):306–320

Özyurt M, Al-Aasm IS, Kirmaci MZ (2019b) Diagenetic Evolution of Upper Jurassic-Lower Cretaceous Berdiga Formation, NE Turkey: Petrographic and Geochemical Evidence. In: Paleobiodiversity and Tectono-Sedimentary Records in the Mediterranean Tethys and Related Eastern Areas (pp. 175–177). Springer, Cham.

Özyurt M, Kirmaci MZ, Yılmaz İÖ, Kandemir R (2019c) Sedimentological and Geochemical Records of Lower Cretaceous Carbonate Successions Around Trabzon (NE Turkey): Implications for Paleoenvironmental Evolution and Paleoclimatological Conditions of Tethys. In Patterns and Mechanisms of Climate, Paleoclimate and Paleoenvironmental Changes from Low-Latitude Regions (pp. 19–21). Springer, Cham.

Özyurt M, Kırmacı MZ, Al-Aasm I, Hollis C, Taslı K, Kandemir R (2020) REE characteristics of Lower Cretaceous Limestone Succession in Gümüşhane, NE Turkey: implications for Ocean Paleoredox conditions and diagenetic alteration. Minerals 10(8):683

Özyurt M, Kırmacı MZ, Yılmaz İÖ, Kandemir R, Taslı K (2022) Sedimentological and geochemical approaches for determination of the palaeoceanographic and palaeoclimatic conditions of Lower Cretaceous marine deposits in the eastern part of Sakarya Zone. NE Turkey Carbonates Evaporites 37(2):25

Özyurt M, Kandemir R, Yıldızoğlu S (2023) Geochemical characteristics of the Turonian-Coniacian strata: New insight into paleoenvironmental conditions of the Tethys, Eastern Pontides, NE Turkey will be published in Journal of Asian Earth Sciences: X, 10, 100156.

Özyurt M, Kırmacı MZ (under review). Microfacies and geochemistry of Kimmeridgian limestone strata in Eastern Pontide (NE Türkiye): New insight into paleoclimatic and paleoenvironmental conditions. J Depositional Record.

Pedersen TF, Calvert SE (1990) Anoxia vs. productivity: what controls the formation of organic-carbon-rich sediments and sedimentary rocks?. Aapg Bull 74(4):454–466.

Pelin S (1977) Geological study of the area southeast of Alucra (Giresun) with special reference to its petroleum potential. Karadeniz Teknik Universitesi, Yerbilimleri Dergisi, Jeoloji 1:15–20

Pratt LM (1984) Influence of paleoenvironmental factors on preservation of organic matter in Middle Cretaceous Greenhorn Formation, Pueblo. Colorado AAPG Bull 68(9):1146–1159

Qing H, Mountjoy EW (1994) Rare earth element geochemistry of dolomites in the Middle Devonian Presqu'ile barrier, Western Canada Sedimentary Basin: implications for fluid-rock ratios during dolomitization. Sedimentology 41(4):787–804

Quijano ML, Castro JM, Pancost RD, de Gea GA, Najarro M, Aguado R, Rosales J, Martín-Chivelet J (2012) Organic geochemistry, stable isotopes, and facies analysis of the Early Aptian OAE—New records from Spain (Western Tethys). Palaeogeogr Palaeoclimatol Palaeoecol 365:276–293

Ratcliffe K, Wright M, Montgomery P, Palfrey A, Vonk A, Vermeulen J, Barrett M (2010) Application of chemostratigraphy to the Mungaroo Formation, the Gorgon field, offshore northwest Australia. APPEA J 50(1):371–388

Redivo HV, Mizusaki AM, Santana AV (2019) REE patterns and trustworthiness of stable carbon isotopes of Salitre Formation, Irecê Basin (Neoproterozoic), São Francisco Craton. J S Am Earth Sci 90:255–264

Reynard B, Lécuyer C, Grandjean P (1999) Crystal-chemical controls on rare-earth element concentrations in fossil biogenic apatites and implications for paleoenvironmental reconstructions. Chem Geol 155(3–4):233–241

Rimmer SM (2004) Geochemical paleoredox indicators in Devonian-Mississippian black shales, central Appalachian Basin (USA). Chem Geol 206(3–4):373–391

Riquier L, Tribovillard N, Averbuch O, Devleeschouwer X, Riboulleau A (2006) The Late Frasnian Kellwasser horizons of the Harz

Mountains (Germany): two oxygen-deficient periods resulting from different mechanisms. Chem Geol 233(1–2):137–155
Robinson A, Spadini G, Cloetingh S, Rudat J (1995) Stratigraphic evolution of the Black Sea: inferences from basin modelling. Mar Pet Geol 12(8):821–835
Rohais S, Hamon Y, Deschamps R, Beaumont V, Gasparrini M, Pillot D, Romero-Sarmiento MF (2019) Patterns of organic carbon enrichment in a lacustrine system across the KT boundary: insight from a multi-proxy analysis of the Yacoraite Formation, Salta rift basin. Argentina Int J Coal Geol 210:103208
Roy DK, Roser BP (2013) Climatic control on the composition of Carboniferous-Permian Gondwana sediments, Khalaspir basin. Bangladesh Gondwana Res 23(3):1163–1171
Sageman BB, Murphy AE, Werne JP, Ver Straeten CA, Hollander DJ, Lyons TW (2003) A tale of shales: the relative roles of production, decomposition, and dilution in the accumulation of organic-rich strata, Middle-Upper Devonian. Appalachian Basin Chem Geol 195(1–4):229–273
Sanchez-Hernandez Y, Florentin JMM (2016) The influence of regional factors in the expression of oceanic anoxic event 1a (OAE1a) in the semi-restricted Organyà Basin, south-central Pyrenees, Spain. Palaeogeogr Palaeoclimatol Palaeoecol 441:582–598
Sahoo SK, Planavsky NJ, Kendall B, Wang X, Shi X, Scott C, Anbar AD, Jiang G (2012) Ocean oxygenation in the wake of the Marinoan glaciation. Nature 489(7417):546–549
Satish-Kumar M, Shirakawa M, Imura A, Otsuji-Makino N, Imanaka-Nohara R, Malaviarachchi SPK, Fitzsimons ICW, Sajeev K, Grantham GH, Windley BF, Hokada T, Takahashi T, Shimoda G, Goto KT (2021) A geochemical and isotopic perspective on tectonic setting and depositional environment of Precambrian meta-carbonate rocks in collisional orogenic belts. Gondwana Res 96:163–204
Scott C, Lyons TW, Bekker A, Shen YA, Poulton SW, Chu XL, Anbar AD (2008) Tracing the stepwise oxygenation of the Proterozoic ocean. Nature 452(7186):456–459
Şen C (2007) Jurassic volcanism in the Eastern Pontides: is it rift related or subduction related? Turkish J Earth Sci 16(4):523–539
Sengör AC, Yilmaz Y, Ketin I (1980) Remnants of a pre–Late Jurassic ocean in northern Turkey: fragments of Permian-Triassic Paleo-Tethys? Geol Soc Am Bull 91(10):599–609
Shields GA, Webb GE (2004) Has the REE composition of seawater changed over geological time?. Chem Geol 204(2004):103–107
Shields G, Stille P (2001) Diagenetic constraints on the use of cerium anomalies as palaeoseawater redox proxies: an isotopic and REE study of Cambrian phosphorites. Chem Geol 175(1–2):29–48
Sholkovitz ER, Landing WM, Lewis BL (1994) Ocean particle chemistry: the fractionation of rare earth elements between suspended particles and seawater. Geochim Cosmochim Acta 58(6):1567–1579
Sholkovitz E, Shen GT (1995) The incorporation of rare earth elements in modern coral. Geochim Cosmochim Acta 59(13):2749–2756
Socorro J, Maurrasse FM (2019) Continuous accumulation of organic matter-rich sediments associated with Oceanic Anoxic Event 1a in the El Pujal section, Organyà Basin, Catalunyà Spain and its relation to episodic dysoxia. Cretac Res 95:225–251
Socorro J, Maurrasse FJMR, Sanchez-Hernandez Y (2017) Characterization of the negative carbon isotope shift in segment C2, its global implications as a harbinger of OAE1a. Sci China Earth Sci 60:30–43
Swart PK, Cantrell DL, Westphal H, Handford CR, Kendall CG (2005) Origin of dolomite in the Arab-D reservoir from the Ghawar Field, Saudi Arabia: evidence from petrographic and geochemical constraints. J Sediment Res 75(3):476–491
Tasli K, Özer E, Yilmaz C (1999) Biostratigraphic and environmental analysis of the Upper Jurassic-lower cretaceous carbonate sequence in the Başoba Yayla Area (Trabzon, NE Turkey). Turkish J Earth Sci 8(2):125–135
Taslı K (1997) Doğu Pontidlerde Malm volkanizmasının varlığına ilişkin stratigrafik ve paleontolojik veriler. İstanbul Üniversitesi Yerbilimleri Dergisi 1991–1992–1993, C. 8, S. 1–2–3, s. 95–101, İstanbul.
Taslı K (1991) Stratigraphy, paleogeography, and micropaleontology of Upper Jurassic–Lower Cretaceous carbonate sequence in the Gümüshane and Bayburt areas (NE Turkey) (Doctoral dissertation, Ph. D. thesis, Karadeniz Technical University, Trabzon (unpublished)(in Turkish with English abstract)).
Taylor SR, McLennan SM (1985) The continental crust: its composition and evolution (p. 312) Oxford
Temizel İ, Arslan M, Ruffet G, Peucat JJ (2012) Petrochemistry, geochronology and Sr–Nd isotopic systematics of the Tertiary collisional and post-collisional volcanic rocks from the Ulubey (Ordu) area, eastern Pontide, NE Turkey: implications for extension-related origin and mantle source characteristics. Lithos 128:126–147
Topuz G, Altherr R, Schwarz WH, Dokuz A, Meyer HP (2007) Variscan amphibolite-facies rocks from the Kurtoğlu metamorphic complex (Gümüşhane area, Eastern Pontides, Turkey). Int J Earth Sci 96:861–873
Traill RJ, Lachance GR (1966) A practical solution to the matrix problem in X-ray analysis. II. Application to a multicomponent alloy system. Can Spectrosc 11:63–71.
Tribovillard N, Algeo TJ, Lyons T, Riboulleau A (2006) Trace metals as paleoredox and paleoproductivity proxies: an update. Chem Geol 232(1–2):12–32
Tucker ME, Wright VP (2009) Carbonate sedimentology. Wiley, New York
Türk-Öz E, Özyurt M (2019) Palaeoenvironment reconstruction and planktonic foraminiferal assemblages of Campanian (Cretaceous) carbonate succession, Çayırbağ area (Trabzon, NE Turkey). Carbonates Evaporites 34:419–431
Veizer J (2018) Trace elements and isotopes in sedimentary carbonates. In Carbonates (pp. 265–300). De Gruyter.
Veizer J, Hoefs J (1976) The nature of O18/O16 and C13/C12 secular trends in sedimentary carbonate rocks. Geochim Cosmochim Acta 40(11):1387–1395
Veizer J, Ala D, Azmy K, Bruckschen P, Buhl D, Bruhn F, Carden GAF, Diener A, Ebneth S, Godderis Y, Jasper T, Korte C, Pawellek F, Podlaha OG, Strauss H (1999) 87Sr/86Sr, δ13C and δ18O evolution of Phanerozoic seawater. Chem Geol 161(1–3):59–88
Vincent SJ, Guo L, Flecker R, BouDagher-Fadel MK, Ellam RM, Kandemir R (2018) Age constraints on intra-formational unconformities in Upper Jurassic-Lower Cretaceous carbonates in northeast Turkey; geodynamic and hydrocarbon implications. Mar Pet Geol 91:639–657
Wang Y, Liu H, Song G, Hao X, Zhu D, Zhu D (2018a) Formation mechanism of carbonates in the lacustrine muddy shale and it implication for shale oil and gas: a case study of source rocks in Member 4 and Member 3 of Shahejie Formation. Dongying Sag Petrol Res 3(3):248–258
Wang Z, Wang J, Fu X, Zhan W, Armstrong-Altrin JS, Yu F, Feng X, Song C, Zeng S (2018b) Geochemistry of the Upper Triassic black mudstones in the Qiangtang Basin, Tibet: implications for paleoenvironment, provenance, and tectonic setting. J Asian Earth Sci 160:118–135
Waples DW (2013) Geochemistry in petroleum exploration. Springer, Cham

Webb GE, Kamber BS (2000) Rare earth elements in Holocene reefal microbialites: a new shallow seawater proxy. Geochim Cosmochim Acta 64(9):1557–1565

Wu J, Liang C, Yang R, Xie J (2021) The significance of organic matter–mineral associations in different lithofacies in the Wufeng and longmaxi shale-gas reservoirs in the Sichuan Basin. Mar Pet Geol 126:104866

Xu C, Shan X, He W, Zhang K, Rexiti Y, Su S, Liang C, Zou X (2021) The influence of paleoclimate and a marine transgression event on organic matter accumulation in lacustrine black shales from the Late Cretaceous, southern Songliao Basin, Northeast China. Int J Coal Geol 246:103842

Xu Y, Lun Z, Pan Z, Wang H, Zhou X, Zhao C, Zhang D (2022) Occurrence space and state of shale oil: a review. J Petrol Sci Eng, 110183.

Zhang KJ, Li QH, Yan LL, Zeng L, Lu L, Zhang YX, Hui J, Jin X, Tang XC (2017) Geochemistry of limestones deposited in various plate tectonic settings. Earth Sci Rev 167:27–46

Zhang K, Liu R, Liu Z, Li L, Wu X, Zhao K (2020) Influence of palaeoclimate and hydrothermal activity on organic matter accumulation in lacustrine black shales from the Lower Cretaceous Bayingebi Formation of the Yin'e Basin, China. Palaeogeogr Palaeoclimatol Palaeoecol 560:110007